Implementation of Externally Imposed Flow in Stellarator Plasma

Master Thesis
submitted to the
Escola Tècnica d'Enginyeria de Telecomunicació de Barcelona
Universitat Politècnica de Catalunya
by

Jose Miralles

In partial fulfillment
of the requirements for the master in
Engineering Physics

Advisor: Shimpei Futatani and Jordi Marti Rabassa
Barcelona, Date 07/2022

Contents

List of Figures

Revision history and approval record

Revision	Date	Purpose
0	dd/mm/yyyy	Document creation
1	dd/mm/yyyy	Document revision

DOCUMENT DISTRIBUTION LIST

Name	e-mail
[Student name]	
[Project Supervisor 1]	
[Project Supervisor 2]	

Written by:		Reviewed and approved by:	
Date	dd/mm/yyyy	Date	dd/mm/yyyy
Name	Xxxxxxx yyyyyyy	Name	Zzzzzzz Wwwwwww
Position	Project Author	Position	Project Supervisor

Abstract

Numerical simulations of non-linear MHD in a stellarator plasma have been performed using MIPS code. During the project, the preliminary approach of the implementation of an externally imposed flow in MIPS code has been carried out. The effect of the imposed flow has been observed by comparison between the simulations of with and without the flow. The implementation of the tested shear profiles show a direct effect on the velocity and magnetic field MHD modes. Three different profiles of imposed shear flow have been compared. The analysis shows that the introduction of sheared flow within the plasma causes premature excitation in the linear modes of the magnetic field, ultimately causing a potentially more unstable plasma than the non-imposed flow cases.

1 Introduction

For the last several decades, human energy demands have been increasing exponentially due to the accelerated general advancement of technology. From the commercialization of cars and airplane flights to the current programs and robotics we utilize to automatize and aid in multiple fields, most of these novelties come with greater energy requirements [1]. These needs have been met with scrambled energy sources, from the hopeful yet imperfect renewable energies to the harmful fossil fuels, the far-off warnings of global climate change have always been neglected or ignored due to political or economic reasons.[2] Even though there has been much effort to avoid future catastrophic consequences, historic and recent trends in energy use show that reliance on carbon and fossil fuels will not diminish soon (see fig. 1).

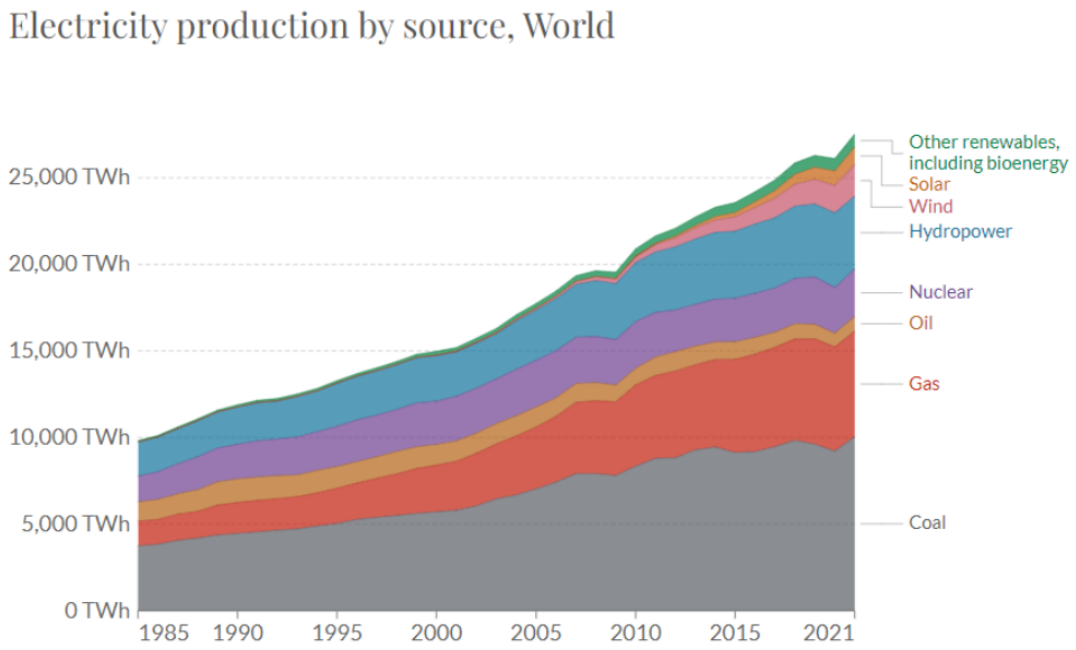

Figure 1: World fuel consumption over the years along the specific types of energy sources [3]

Myriad of current and past evidence signify the urgency of the matter: the millions of acres being wiped out by fires, flooding of several cities and towns, yearly record-breaking temperatures. Improvements for current renewable energies seem promising in the long run, yet these would never be able to substitute harmful energy sources in time unless replaced and implemented successfully in mass. Almost as in an all or nothing situation, many hopes lie with the success of nuclear fusion.

Historically, nuclear fusion has been around for over 70 years. However, efforts have not been able to surpass the obstacles involved in achieving commercial nuclear fusion. Aside from requiring a colossal amount of input energy to kick-start the reaction (not even considering the energy required to run the power plant itself), the reaction must be sustained for long enough so as to extract more energy than the input. This is what would make

the entire venture worthwhile and is what is measured and referred to as the energy gain value or 'Q' factor:

$$Q = \frac{P_{fusion}}{P_{heat}} \tag{1}$$

Having Q to be larger or equal to 1 is what is known as 'break-even', a goal yet unachieved. Since the advent of nuclear fusion reactors, there have been multiple refinements in reactor design and configuration, yet none have reached break-even. Figure 2 shows some of the most relevant fusion reactors over the years measured by their 'triple product': a measurement of their overall effectiveness considering the reached plasma temperature and confinement time from a starting density. The record for this value for a magnetically confined plasma is, as of the date of this paper, currently held by the JET fusion reactor in the UK with a Q value of 0.67 [4]. However, currently undergoing its final stages of construction in France is ITER, an international project harboring the efforts of 35 nations with collaborated investment of billions of dollars [4]. The project will yield the largest fusion reactor expected to have a Q value of at least 10, set to hopefully prove the possibility for a future powered by fusion.

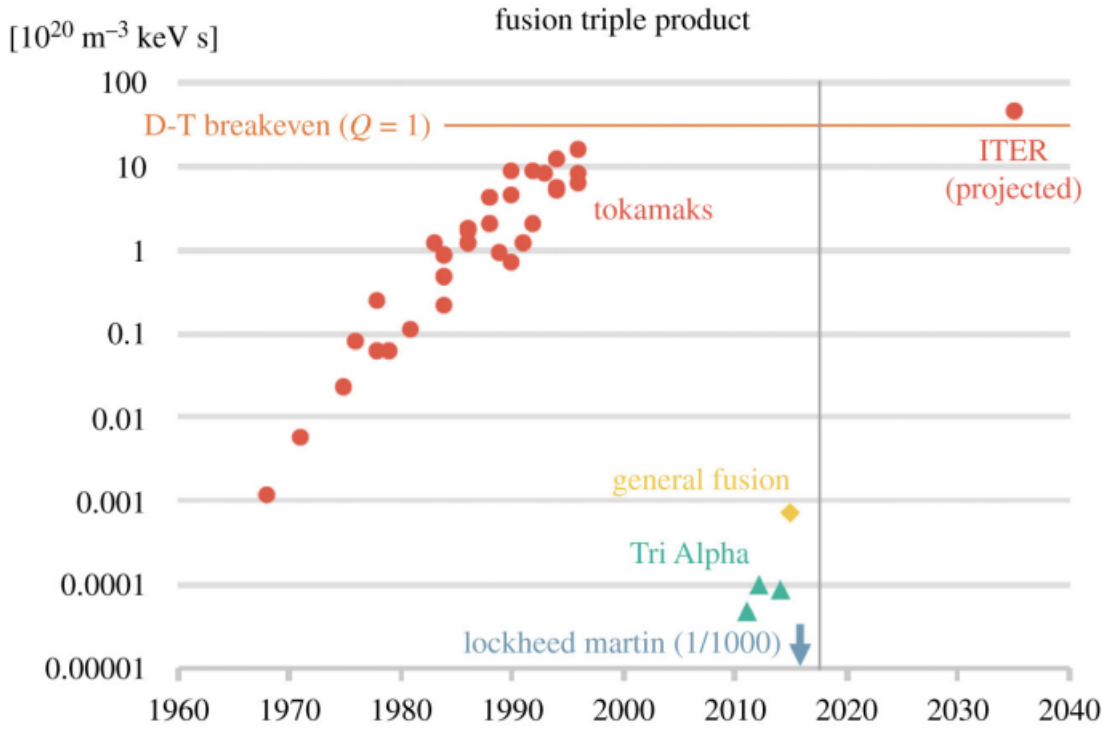

Figure 2: Nuclear fusion reactors throughout the years. Here, the term 'Triple Product' is indicative of the overall effectiveness of the reactor as this measurement takes into account the plasma's density, temperature, and confinement time [5]

1.1 What is Nuclear Fusion?

Where nuclear fission is the splitting of heavy atoms (such as Uranium with atomic number 92), nuclear fusion is the fusing of light atoms (like Hydrogen with atomic number 1). With the right conditions, two atoms become fused together due to the strong force which only acts at distances in the order of nucleon radii [6]. Achieving nuclear fusion means surpassing the Coulomb barrier imposed by the protons in the nucleon of the atoms. The conditions for this to happen naturally can only be found in a star's core, having the right mixture of density, pressure, and gravitational force there is enough energy for individual atoms to surpass this barrier and fuse by the strong force.

In theory, any two elements can fuse, but the more ions comprising the atoms the more energy is required to surpass the resulting Coulomb barrier and the less net energy is gained. Stars are fueled by fusion reactions (up until Iron, where after there is no more energy gained from the fusion reaction), the energy coming directly from the difference between the initial two atoms and the resulting fused atom. With Einstein's famous formula $E = mc^2$, just one kilogram of mass would yield a colossal $9\text{x}10^{16}$ Joules of energy. The sun burns around 350 billion tonnes a day [7] which equals $3.15\text{x}10^{31}$ Joules of energy. Capturing all energy released from the Sun within just 0.2 nanoseconds would suffice the yearly world energy consumption of $5.8\text{x}10^{14}$ Joules [8]. While large amounts of the Sun's energy does reach Earth via photons, this energy gets massively filtered and only a small fraction is captured and stored by our current technology. Naturally, to be able to produce energy as the stars do, directly from the source, is extremely attractive.

Currently, the best fuel candidates for nuclear fusion on Earth are two Hydrogen isotopes, Deuterium (D) and Tritium (T), since their cross-section (probability of fusion as temperature increases) peaks the highest at the lowest temperatures out of all other combinations (see Figure 3) [6]. This reaction would carry out as

$$D + T \rightarrow {}^4He + n + 17.6MeV$$

To achieve nuclear fusion on Earth, the temperature required is 150 million degrees Celsius, 10 times more than the Sun's core [9]. The reason for this is that on Earth the conditions are lacking: not enough density or pressure, so, to compensate, higher temperatures are necessary to increase the likelihood of collision and fusion between the atoms. Though achieved, confining the immensely hot plasma for a sufficient period of time has proven to be the main obstacle preventing commercial nuclear fusion power plants and break-even as plasmas are highly unstable and difficult to confine. Naturally, the longer the confinement, the more fusion reactions would occur and hence the more energy would be extracted from the initial fuel.

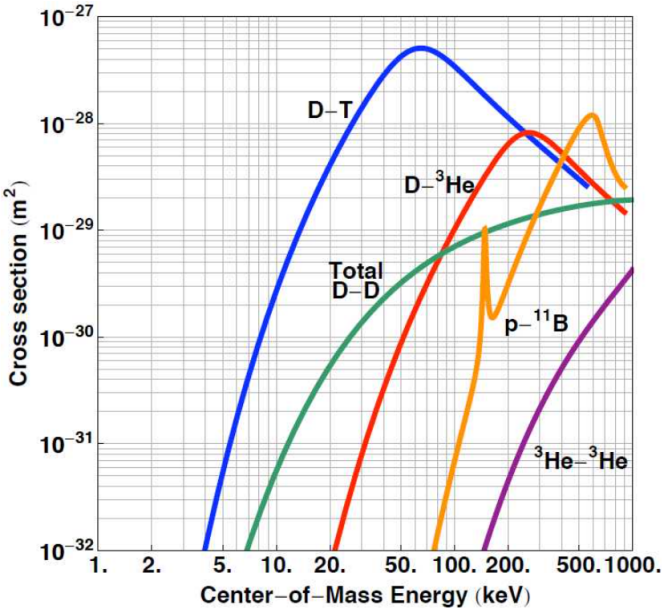

Figure 3: Graph showing the peaks of different atomic combinations of fuel for nuclear fusion reactions as temperature increases. D-T reactions are shown to be clearly the most effective candidate. [10]

1.2 Tokamaks and Stellarators

There are many ways one could achieve a fusion reaction on Earth: inertial confinement, inertial electrostatic confinement, beam-beam or beam-target fusion,... Yet, the most popular and promising method is thermonuclear fusion, which is the method described in the previous section and which most closely emulates stars. Considering that here the plasma is extremely hot and must be kept this way, the only way to confine it without it touching anything would be by magnetically confining it. Even though the plasma is ionized and electrically charged, unfortunately electrical confinement is not possible since Laplace's equation, $\nabla^2 = 0$, implies electric fields give no equilibrium points [11]. However, methods such as the mentioned inertial electrostatic confinement utilize the inertial motion from the gradient of the potential to achieve fusion reactions.

Currently, several different designs for magnetic confinement devices exist. The most popular is the tokamak. The tokamak's design is described by a toroidal shape and is the design that has seen the most success in performing effective fusion reactions (JET and ITER both use this design) [4, 9]. Similar to the tokamak, the next most popular and promising design is the so-called stellarator. Keeping the toroidal shape of the tokamak, the main difference giving this design its main profile is the twisting of the magnetic field along its contour (see fig. 4). The main advantage of stellarators over tokamaks is that these produce a steady state magnetic field and they lack instabilities and disruption from the induction of electric currents inside the plasma [12]. This means that there is an entire problem in keeping the plasma stable simply avoided by design. Unfortunately, stellarators are significantly more difficult to engineer and manufacture since their oddly

shaped magnets must be made with millimeter precision. Even then, there are stellarators in existence such as the Wendelstein 7-X in Germany and the HSX in the United States [13, 14].

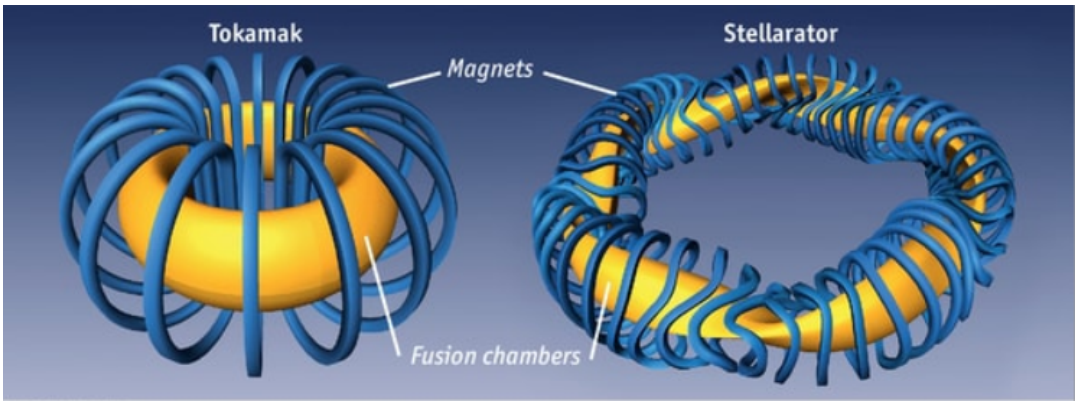

Figure 4: Comparison between the shape of a tokamak and a stellarator [15]

One of the most important stellarators in the world, though, is the Large Helical Device (LHD) in Toki, Japan [16] (see fig. 5). This is one of the leading stellarator fusion reactors in helical plasma research, employing a Heliotron magnetic field configuration which, in addition to the characteristical twisted magnetic field, uses poloidal coils to produce a vertical magnetic field to control surface characteristics of the plasma. The reactor is able to produce magnetic fields of 3 Tesla, has a heating power of 36 MW, and can hold a plasma volume of $30m^3$ [16].

Furthermore, plasma parameters at which LHD operates is with a density of 100 trillion ions per cm^3 and at a temperature of 120 million degrees Celsius [16]. The standard major radius of the magnetic axis is located at a value of 3.75 m and has shown good, stable performance for years, but LHD has been engineered so that it is flexible enough that fields can be adjusted to test other configurations [17]. With simulations, improvements for stable configurations can be tested with relative tranquility that it can be realistically achieved using LHD.

Figure 5: Inside the LHD reactor [4]

2 Magnetohydrodynamics

Considering that plasma is an electrically conductive fluid, to describe these objects one must rely on Magnetohydrodynamics (MHD) [18]. The field is extremely complex, governed by an extensive set of equations to which only few cases have exact solutions; the equations being a marriage between Maxwell´s formulations and Hydrodynamics. This complexity is due to the fact that electrically conductive fluids such as plasmas get electrical currents induced from a magnetic field which then polarizes the fluid which then in turn induces another magnetic field from itself and so on. Microscopically, it is nearly impossible to realistically describe with accuracy the dynamics of every single particle due to the other ones and itself. However, macroscopically the dynamics can be determined to an acceptable accuracy.

2.1 Ideal and Non-Ideal MHD

Ideally, plasma will have no resistivity, viscosity, thermal conduction, or radiative cooling, meaning that there is no dissipation of energy in the system. However, introducing dissipative forces into the ideal equations result in the following manner:

- Mass Continuity Equation

$$\frac{\partial \rho}{\partial t} + \nabla \cdot (\rho \mathbf{V}) = 0 \tag{2}$$

- Energy Equation

$$\boxed{\frac{\rho^{\gamma}}{\gamma - 1}} \frac{d}{dt}\left(\frac{P}{\rho^{\gamma}}\right) = \boxed{-\mathcal{L}} \tag{3}$$

- Euler´s Equation

$$\rho \frac{\partial \mathbf{V}}{\partial t} + \boxed{\rho(\mathbf{V} \cdot \nabla)\mathbf{V}} = -\nabla P - \frac{1}{\mu}\mathbf{B} \times (\nabla \times \mathbf{B}) + \boxed{\mathcal{F}} \tag{4}$$

- Induction Equation

$$\frac{\partial \mathbf{B}}{\partial t} = \nabla \times (\mathbf{V} \times \mathbf{B}) + \boxed{\eta \nabla^2 \mathbf{B}} \tag{5}$$

where ρ is the density, t is the time, $\mathbf{V}$ is the plasma velocity, P is the pressure, $\mathbf{B}$ is the magnetic field, γ the ratio of specific heats usually taken to be 5/3, $\mathcal{F}$ is an external force acting on a unit volume of the plasma, η the magnetic diffusivity, and $\mathcal{L}$ the energy gain/loss function. The boxed sections of the equations are the additional terms added when considering dissipative forces unto the ideal equations. It is to note that these set of equations have been derived from a single-fluid model of the plasma, that is, by considering that the plasma is macroscopically one body comprised of one heterogeneous fluid. From these equations, one can begin to approach the realistic behavior of plasmas when succumbed unto different conditions and configurations now regarding the fusion device in question.

For MHD equilibrium the conditions are

$$\mathbf{V} = 0, \qquad \frac{d}{dt} = 0, \tag{6}$$

which lead to the magnetostatic equation

$$\nabla P_0 + \frac{1}{\mu_0}\mathbf{B}_0 \times (\nabla \times \mathbf{B}_0) = 0 \tag{7}$$

From the ideal model, even though unrealistic, the main equilibrium points are illustrated by the magnetostatic equation 7. These equations are helpful in determining the required magnetic field evolution as time passes for providing a stable magnetic equilibrium to the plasma for a given initial pressure. The main parameters that will account for plasma equilibrium are total pressure, magnetic pressure, and magnetic tension [18, 19, 20].

2.2 Plasma Confinement and MHD Equilibrium

The main goal is to keep the hot plasma from escaping the fusion reactor. Figure 6a denotes the setting of the plasma within the reactor and figure 6b the required pressure profile for successful plasma confinement. With the set of non-ideal MHD equations, a further set of equations can be obtained to illustrate the key parameters needed to control and achieve a stable plasma. The key equations that dictate plasma equilibrium when assuming static and time-independent values are

$$\mathbf{J} \times \mathbf{B} = \nabla P \tag{8}$$

$$\nabla \times \mathbf{B} = \mu_0 \mathbf{J} \tag{9}$$

$$\nabla \cdot \mathbf{B} = 0 \tag{10}$$

where $\mathbf{J}$ is the current density vector and μ_0 the permeability of free space [18].

Furthermore, the two main aspects of plasma which cause instability within the plasma are the radial pressure which causes the plasma to expand radially outwards and the toroidal forces which are caused by the toroidicity generated by the magnetic fields, making the plasma to also expand radially. To counteract the radial pressure, solutions are to implement a constraining force magnetically also referred to as θ pinch, Z-pinch, or screw pinch depending on the direction of origin or configuration of the source of magnets responsible. Unfortunately, toroidal forces can only be counteracted with Z or screw pinches and require further externally applied electrical fields, adding complexity. However, stellarators were designed just to avoid this problem altogether. Due to the unique twisting of the magnets comprised in its design, toroidal forces are able to balance [18].

The stability of plasma can further be aided by the careful implementation of shear forces. Without these shear forces, eddy vortices begin accumulating on the plasma layers, altering the location of the stable points of the magnetic fields hence causing turbulent flow and instabilities from within the plasma [21]. Shear forces ultimately help counteract the detrimental effects of the arising eddy vortices by breaking up the buildup into smaller pieces as shown in figure 7.

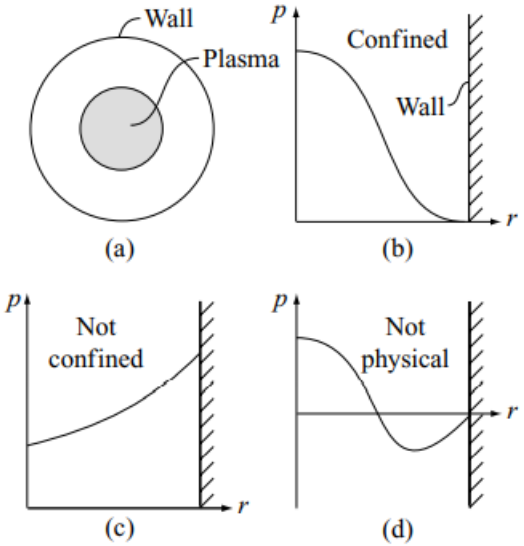

Figure 6: Figure a) shows a contained plasma within the fusion reactor. Figures b) c) and d) show the pressure profiles in different scenarios as seen from within the reactor at a side [18]

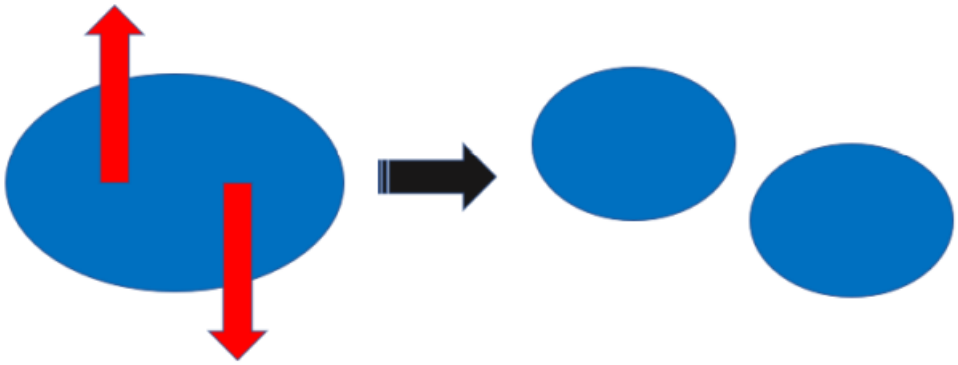

Figure 7: An area with a build up of eddy vortices (denoted by the blue ovals) is split into two by shear forces denoted by the red arrows. The shear force is imposed externally and acts from within the plasma to produce sheared motion.

3 Methodology

To investigate the behaviour of LHD-like plasma when succumbed to different initial parameters, either stable or unstable, the main resource utilized was the Barcelona Supercomputing Center's super computer: MareNostrum [22]. Here, a code containing all equations required to effectively simulate stellarator reactors was executed to study the implementation of the imposing flow equations and their effect on initially unstable configurations of the plasma. Analysis of the output data containing primarily the energy profiles, velocity and magnetic fields, and pressure was conducted by the use of Python scripts and ParaView, a 3D plotting software.

3.1 MHD Infrastructure for Plasma Simulation

For nuclear fusion research, computer simulations are paramount. Aside from helping in refining and developing the leading theory, simulations also provide an essential insight into the model and system itself. Here, important improvements in designs are usually due to the results provided by simulations, which might fine tune certain design choices and parameters demonstrated to be more effective or yield overall better results.

MHD Infrastructure for Plasma Simulation (MIPS) is a code written in FORTRAN language and was developed in Japan for the sole purpose of solving the non-linear MHD equations for nuclear fusion plasma in 3D [23, 24, 25, 26]. As input the code requires the macro-parameters defining the reactor and initial plasma attributes to which the plasma is going to be simulated: major and minor radius of the reactor, plasma density, magnetic field attributes, calculation step, etc... The output of the program is the resulting pressure, velocities, magnetic field, and energies at each step of calculation (see Appendix A). The advantage of MIPS code over most other codes simulating plasma confined in a fusion reactor is the coordinate system it utilizes, a grid-like Cartesian system with cylindrical coordinates which can be manipulated to simulate almost any reactor's geometry as seen in figure 8. Even though this flexibility comes with the disadvantage of non-specialization, it is a design which allows for the simulation of stellarators, a configuration rarely able to be simulated by other codes due to the complexity involved in the model.

The code simulates the plasma assuming charge-neutrality and incompressibility. The modeled dynamics are illustrated by the following set of equations:

$$\frac{\partial \rho}{\partial t} + \nabla \cdot (\rho \mathbf{V}) = \nabla \cdot (D_\perp \rho) \tag{11}$$

$$\rho \left(\frac{\partial \mathbf{V}}{\partial t} + \mathbf{V} \cdot \nabla \mathbf{V} \right) = -\nabla P + \mathbf{J} \times \mathbf{B} + \frac{4}{3}[v\rho \nabla \cdot \mathbf{V}] - \nabla \times (v\rho \boldsymbol{\omega}) \tag{12}$$

$$\frac{\partial P}{\partial t} + \nabla \cdot (P\mathbf{V}) + (\Gamma - 1) P \nabla \cdot \mathbf{V} = \nabla \cdot (\chi_\perp \nabla P) + \nabla \cdot \left[\mathbf{B} \left(\frac{\chi_\parallel}{B^2} (\mathbf{B} \cdot \nabla) P \right) \right] \tag{13}$$

$$\frac{\partial \mathbf{B}}{\partial t} = -\nabla \times \mathbf{E} \tag{14}$$

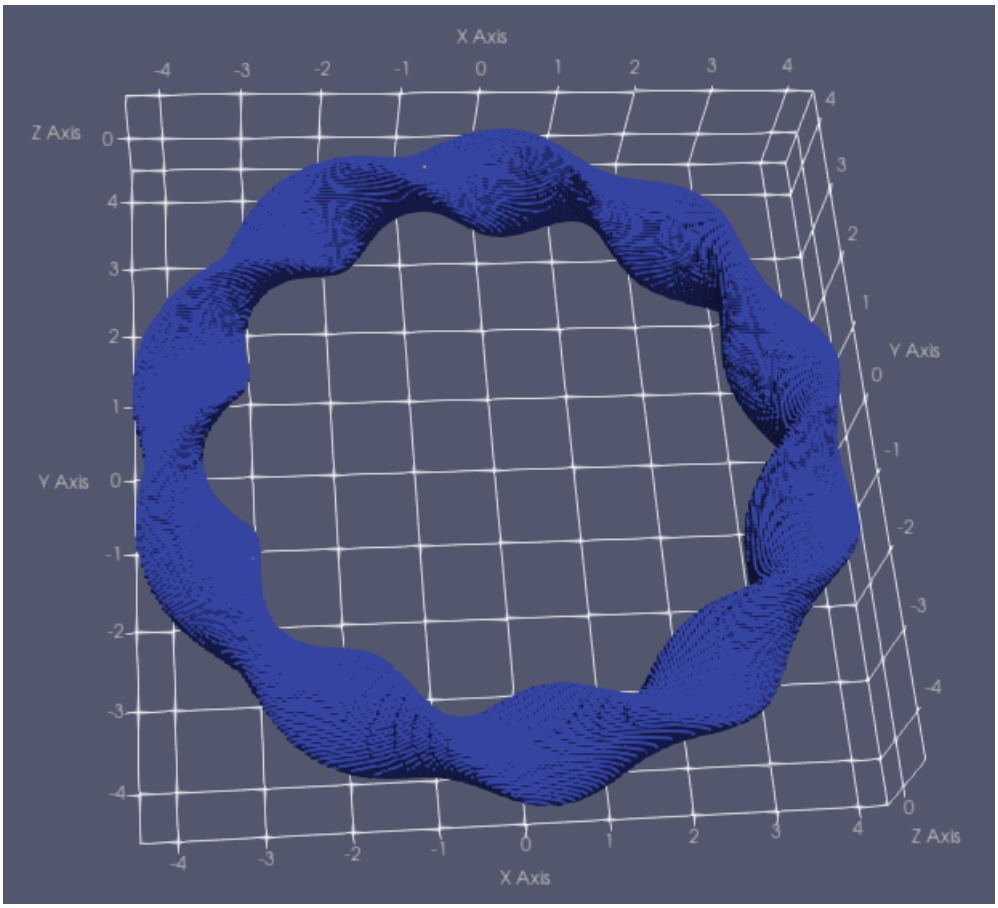

Figure 8: Simulated stellarator shape showing based cartesian grid

$$\mathbf{E} + \mathbf{V} \times \mathbf{B} = \eta(\mathbf{J} - \mathbf{J}_{eq}) \tag{15}$$

where $\chi_{\parallel}$ and $\chi_{\perp}$ are the parallel and perpendicular heat conductivities respectively, v is the viscosity, η the resistivity, $D_{\perp}$ the perpendicular electrical displacement, Γ the adiabatic constant for ideal gas equalling $\frac{5}{3}$, and $\boldsymbol{\omega} = \nabla \times \mathbf{V}$ the vorticity [24, 23]. The equations include slight additions and variances from the set of equations shown in the MHD section for code simulation adaptation, but both spurn out from the same theory. These equations are dynamically solved using cylindrical coordinates in a cartesian grid, hence giving the flexibility mentioned previously which allows for the simulation of stellarators.

MIPS utilizes various methods for the calculation of different aspects of the plasma being simulated. 4th-order central finite difference method is used to compute spatial derivatives, 4th-order Runge-Kutta method is used to compute time evolution, and 3rd-order upwind scheme (Kawamura–Kuwabara scheme) is used to compute convection terms which avoid oscillating numerical errors [23]. The relevant equations are the following:

4th Order Central Finite Difference Method

$$f^{'}(x) = \frac{-f(x+2h) + 8f(x+h) - 8f(x-h) + f(x-2h)}{12h} + O(h^4) \tag{16}$$

where h is the step length.

4th Order Runge-Kutta Method

$$K_1 = hf(x_n, y_n) \tag{17}$$

$$K_2 = hf(x_n + \frac{h}{2}, y_n + \frac{k_1}{2}) \tag{18}$$

$$K_3 = hf(x_n + \frac{h}{2}, y_n + \frac{k_2}{2}) \tag{19}$$

$$K_4 = hf(x_n + h, y_n + k_3) \tag{20}$$

$$y_{n+1} = y_n + \frac{k_1}{6} + \frac{k_2}{3} + \frac{k_3}{3} + \frac{k_4}{6} + O(h^5) \tag{21}$$

3rd-order Upwind Scheme

$$u\frac{\partial u}{\partial x} \approx u_k \frac{-u_{k+2} + 8(u_{k+1} - u_{k-1}) + u_{k-2}}{12\delta x} + |u_k| \frac{u_{k+2} - 4u_{k+1} + 6u_k - 4u_{k-1} + u_k - 2}{12\delta x} \tag{22}$$

Furthermore, MIPS calculates the magnetic, thermal, kinetic, and total energy of the system in the following manner:

$$E_{kinetic} = \int_{R_{min}}^{R_{max}} \frac{1}{2}\rho \mathbf{r}(V^2)\,\mathrm{d}\mathbf{r} \tag{23}$$

$$E_{magnetic} = \int_{R_{min}}^{R_{max}} \frac{1}{2}\mathbf{r}B^2\,\mathrm{d}\mathbf{r} \tag{24}$$

$$E_{thermal} = \int_{R_{min}}^{R_{max}} \mathbf{r}\frac{P}{\gamma - 1}\,\mathrm{d}\mathbf{r} \tag{25}$$

$$E_{total} = E_{kinetic} + E_{magnetic} + E_{thermal} \tag{26}$$

The tracking of the total energy and its sub-constituents serves primarily to keep track of the general status of the plasma and whether it is stable or unstable.

Additionally, pressure can be obtained in the spirit of figure 6 where the pressure can be seen varying with respect to the radial position. Pressure is indicative of position within the plasma.

3.2 Sheared Flow

In a real experiment, sheared flow can be implemented into the plasma primarily by the introduction of radially localized DC electric fields [27]. The response of the plasma itself to this externally imposed electric field resulting in the type of sheared flow is determined mainly by the Debye length of the plasma. Furthermore, the introduction of sheared flow vastly alters the eigenmode structure of the overall equilibrium attributes of the plasma, including velocity, pressure, and magnetic modes and gradients. It is known that strong sheared flows can mitigate instabilities within the plasma, whereas small amplitude sheared flows might be either helpful or detrimental [28].

One important thing to consider, though, is the introduction of energy that imposing shear causes. Experimentally, results of imposed sheared flows are generally extremely sensitive, as these can have large variations in plasma behavior dependent on small differences in the initial experiment setup [29, 27].

4 Results

Previous to running any simulations, the main physical parameters to establish are viscosity (ν_0), resistivity (η_0), diffusivity of density (ν_{N0}), and perpendicular thermal diffusivity (χ_0). These predetermine the simulation in a way by establishing the stability of the plasma as time passes; resistivity destabilizes while the rest act as stabilizers. These simulations were executed with a magnetic field of 3 T, minimum radius of 2.8 m, maximum radius of 4.8 m, and an ion density of $7.7\text{x}10^{19}m^{-3}$.

Internally, MIPS keeps track of the different calculated variables under arbitrary units which then need to be normalized to physical values. The variables to be normalized are time, pressure, density, and temperature. To normalize time the characteristic Alfvén velocity of the simulation configuration must be used, resulting in the following two equations:

$$V_A = \frac{B_0}{\sqrt{\mu_0 \rho_0}} \tag{27}$$

$$t_{real}[s] = t_{MIPS}\left(\frac{R_0}{V_A}\right) \tag{28}$$

where μ_0 is magnetic permeability, ρ_0 is the initial density of ions, R_0 the major radius minus the minor radius, t is time, B_0 the initial magnetic field, and V_A the Alfvén velocity. All simulations presented were ran with an internal time step of $1\text{x}10^{-2}$, equalling around 0.04 nanoseconds per single step in real time.

Finally, presented pressure had to be normalized as well. This was done by the use of the following equation:

$$P_{real}[Pa] = \frac{P_{MIPS}B_0^2}{\mu_0} \tag{29}$$

where P is pressure. However, all presented velocities and magnetic field values are represented in arbitrary units (a.u.), not normalized from the resulting data from the simulation.

The main comparison studied in this thesis is between the cases of imposed flow and non-imposed flow stellarator plasma. All of the presented simulation results begin with the pressure profile shown in figures 9 and 10. The fusion plasma has high density, temperature and pressure in the core region, while those quantities are low in the plasma boundary region. The gradients are unavoidable. The gradients of those quantities are the main source of plasma instabilities.

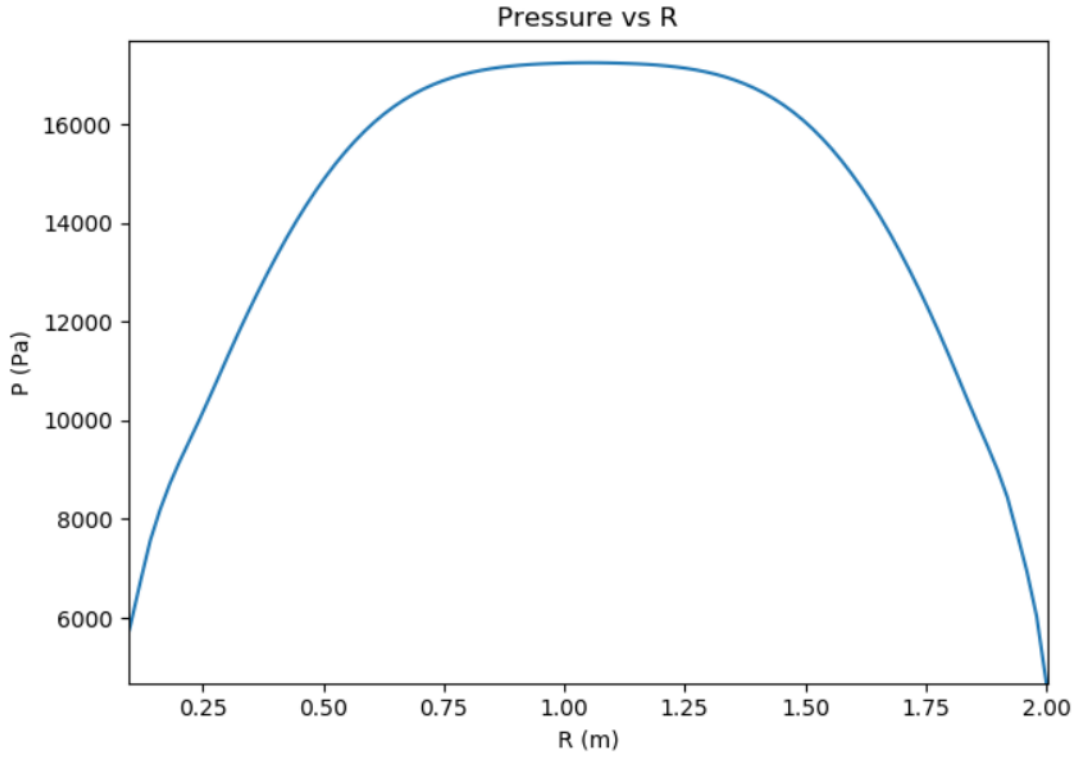

Figure 9: Initial pressure profile where maximum pressure reaches 17 kPa at the core.

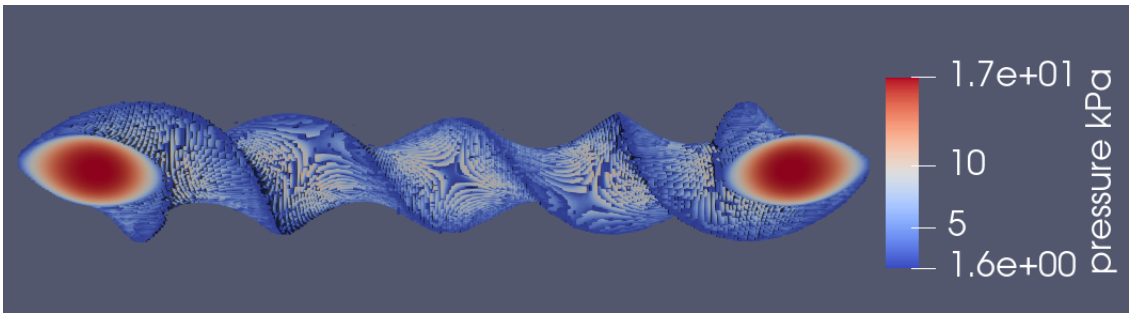

Figure 10: 3D plot of the stellarator´s initial pressure profile at 0.08 μs.

4.1 Non-Imposed Flow Cases

Stable Case

Performing the plasma simulation with stable configuration means decreasing resistivity. Resistivity in plasma is due to Coulomb collisions, acting as energy dissipation in the momentum equation and creating instabilities by giving rise to particle diffusion and magnetic field diffusion [18]. The configuration results in the following initial parameter values, all of which are dimensionless within MIPS:

$$\begin{aligned} \nu_0 &= 1.0 \times 10^{-5} \\ \eta_0 &= 1.0 \times 10^{-7} \\ \nu_{N0} &= 1.0 \times 10^{-6} \\ \chi_0 &= 1.0 \times 10^{-6} \end{aligned} \tag{30}$$

The simulation yields a velocity field spectrum evolution presented in figure 12a where the velocity modes do not grow because the plasma is stable with the plasma parameters shown in equation 30. Furthermore, the initial velocity field is shown in figure 11 where velocity values from within the plasma reach a maximum of 6x10^{-8} a.u. after 0.08 μs. These initial velocities are due to initial perturbations in the system, albeit extremely small.

Unstable Case

The simulation of unstable cases is set primarily by increasing the resistivity. This change would set the initial parameter values as:

$$\begin{aligned} \nu_0 &= 1.0 \times 10^{-5} \\ \eta_0 &= 1.0 \times 10^{-5} \\ \nu_{N0} &= 1.0 \times 10^{-6} \\ \chi_0 &= 1.0 \times 10^{-6} \end{aligned} \tag{31}$$

Initially, the velocity field after 0.08 μs is very similar to the stable case which is shown in figure 11. As shown in figure 12b, the spectrum of the velocity field show an exponential growth at 7.5 μs due the the large value of the resistivity used in the simulation.

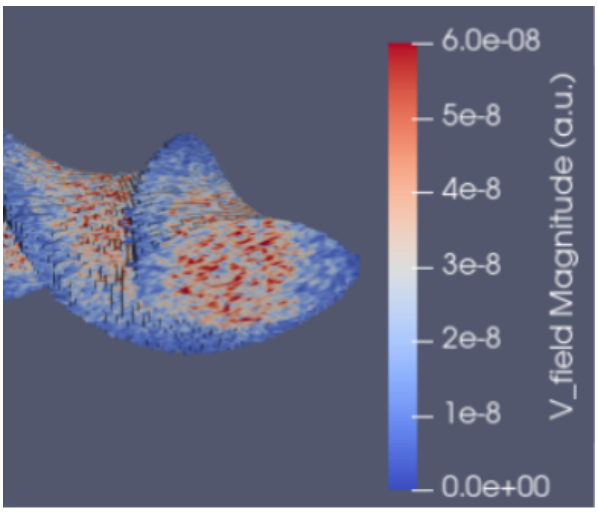

Figure 11: Initial velocity field in a.u. of the stellarator plasma after 0.08 μs

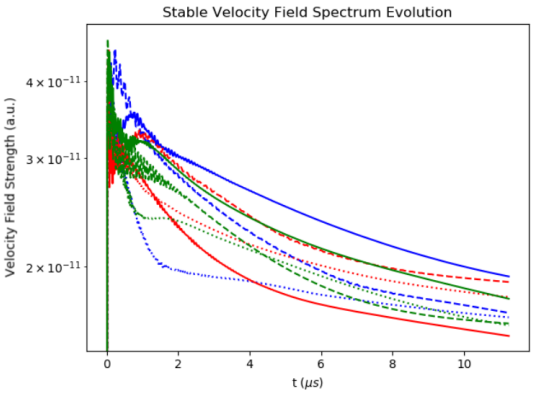

(a) Velocity field modes for the stable case. The velocity values quickly stabilize from an initial value in the order of 4x10^{-11} a.u. to about 2x10^{-11} a.u.

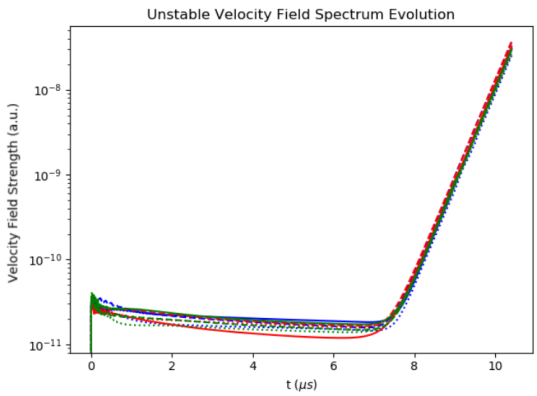

(b) Velocity field modes for the unstable case. The velocity values are shown to be destabilizing after 7.5 μs from an initial value in the order of close to 10^{-11} a.u. to larger than 10^{-8} a.u.

Figure 12: Velocity field spectrum plots of stable and unstable plasma configurations. Blue lines indicate the poloidal mode (m) is 1, red lines are 2, and green lines 3. Dashed lines indicate the toroidal mode (n) is 1, solid lines 2 and dotted lines 3. One red dashed line would indicate the velocity mode for m/n = 2/1

4.2 Imposed Flow Cases

As a preliminary approach to impose an initial sheared velocity within the plasma simulation the following equations were implemented:

$$P_{norm} = 2\pi \left| 1 - \frac{P}{P_{max}} \right| \tag{32}$$

$$u_0 = C \sin(P_{norm}) \tag{33}$$

$$u_0 = C \sin\left(\frac{P_{norm}}{2}\right) \tag{34}$$

The velocity is only initially imposed at the r and z radial coordinates with respect to either the whole angle or half angle sine functions with a normalized pressure peaking at 2π and with an arbitrary amplitude denoted by 'C'. After this implementation on the velocity field calculations, the velocity profile demonstrates sheared flow since the very beginning of the simulation.

The stellarator uses Boozer-coordinates, therefore the poloidal plane is elongated and the poloidal plane rotates according to the toroidal angle. Therefore, the calculation of the magnetic surface is not easy. In order to solve this problem, the pressure profile of the

plasma equilibrium is used. The pressure on the same magnetic flux surface is constant, therefore the normalized pressure can be a replacement to express the magnetic flux surface.

Within MIPS code, the gradients of the pressure are calculated by iterating through the entire initial three-dimensional pressure array. With these, the external initial imposed velocities for sheared flow are calculated with the following two equations:

$$u_r = -u_0 \frac{\frac{\partial P}{\partial z}}{\sqrt{(\frac{\partial P}{\partial r})^2 + (\frac{\partial P}{\partial z})^2}} \tag{35}$$

$$u_z = u_0 \frac{\frac{\partial P}{\partial r}}{\sqrt{(\frac{\partial P}{\partial r})^2 + (\frac{\partial P}{\partial z})^2}} \tag{36}$$

Here, u_r and u_z are the three-dimensional arrays holding the initial imposed velocity values of the r and z axis respectively. The new velocity components, u_r and u_z, follow the velocity fields along the magnetic flux surfaces, i.e. the contour lines of the pressure profile.

Three cases starting from the unstable configuration but varying in amplitude of imposed velocity values and type of imposed flow were studied. The profiles of imposed velocity against normalized pressure are shown for all cases in figure 13.

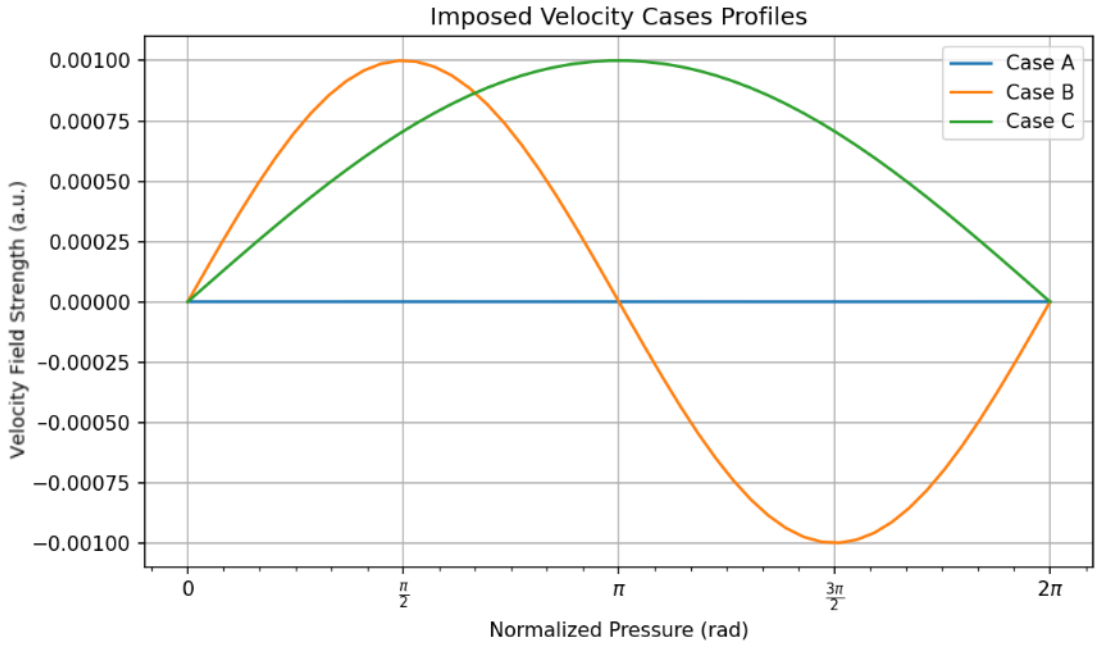

Figure 13: Imposed velocity profiles in a.u. vs normalized pressure for all cases. All cases begin from an unstable configuration. Case A has one full period like case B but with an amplitude of $1x10^{-7}$ and is not discernible in the plot.

Imposed Flow Case A

Case A is defined by the initial u_0 defined by the whole angled sine function (eq. 33) with an amplitude of $1x10^{-7}$ resulting in a small amplitude of imposed sheared velocities. The initial imposed velocity of this case is shown in figure 15a in accordance to its imposed velocity profile and its velocity field spectrum evolution which are shown in figure 14a. Noticeably, the whole angle sine function gives three relevant different areas of velocities encroaching the outer regions of the plasma due to the normalization of the angle corresponding to the pressure profile, where its decay is also in the outer regions of the plasma (refer to fig. 9).

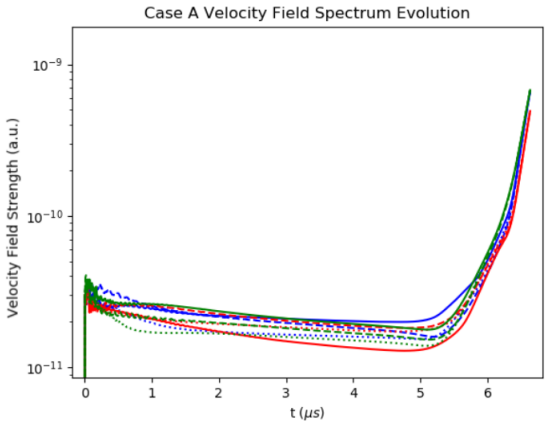

(a) Velocity field spectrum of imposed flow case A reaching 6.6 μs

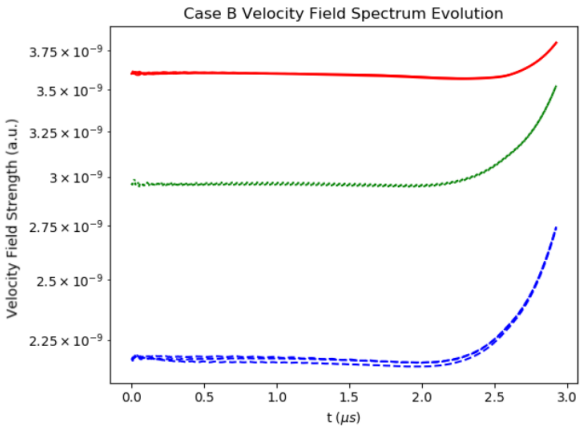

(b) Velocity field spectrum of imposed flow case B reaching close to 3 μs

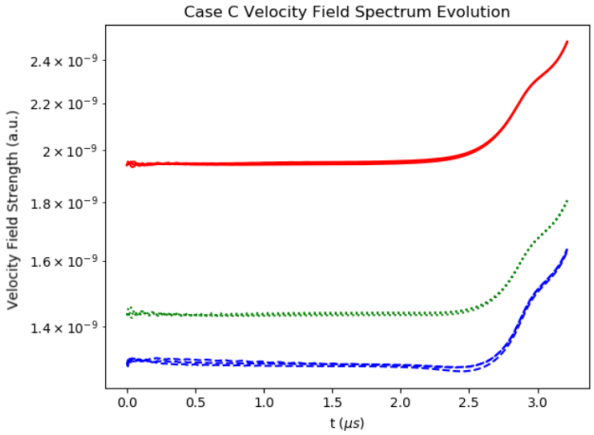

(c) Velocity field spectrum of imposed flow case C reaching close to 3.3 μs

Figure 14: Imposed flow cases velocity field spectrum graphs in a.u. case by case. Blue lines indicate the poloidal mode (m) is 1, red lines are 2, and green lines 3. Dashed lines indicate the toroidal mode (n) is 1, solid lines 2 and dotted lines 3. One red dashed line would indicate the velocity mode for m/n = 2/1

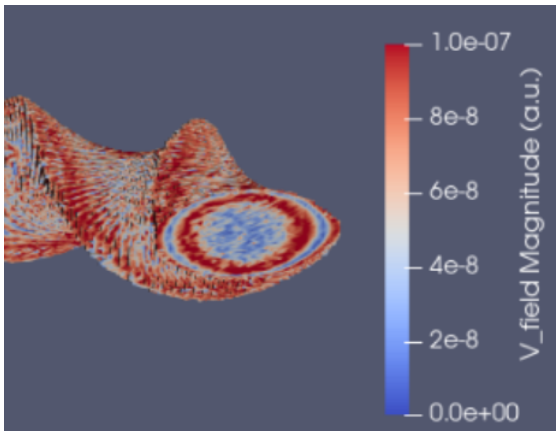

(a) Velocity field of whole angled sine function sheared flow with low amplitude, which means that noise and random fluctuations are more visible. Shown is the plot for case A.

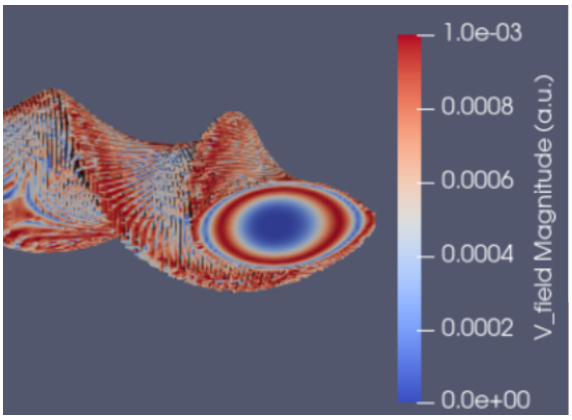

(b) Velocity field of whole angled sine function sheared flow with high amplitude, random fluctuations or noise are not visible. Shown is the plot for case B

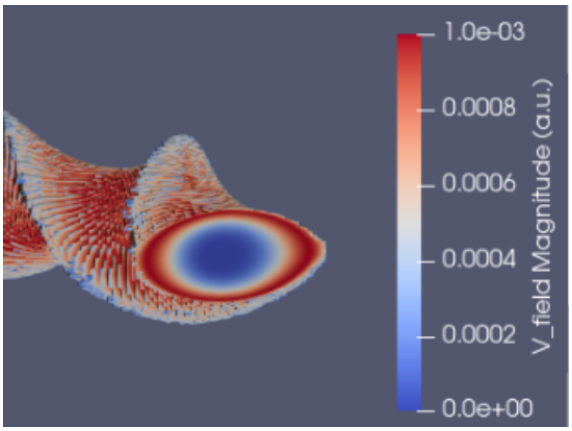

(c) Velocity field of the half angled sine function sheared flow with high amplitude. Shown is the plot for case C.

Figure 15: 3D plots of the stellarator showing the different velocity fields in a.u. after 0.08 μs

Imposed Flow Case B

Case B is defined by the initial u_0 defined by the whole angled sine function (eq. 33) with an amplitude of $1x10^{-3}$. The initial imposed velocity field after 0.08 μs shown in figure 15b displays the three different ringed areas. The amplitude of the shear flow is much larger than the initial perturbation, therefore the profile of the imposed flow is much more clearly visible. The velocity field spectrum evolution is shown in figure 14b.

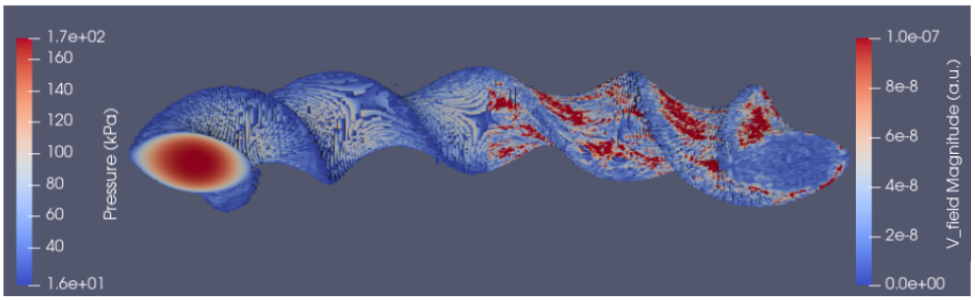

(a) Stable velocity field (right) and pressure (left) at 11.1 μs

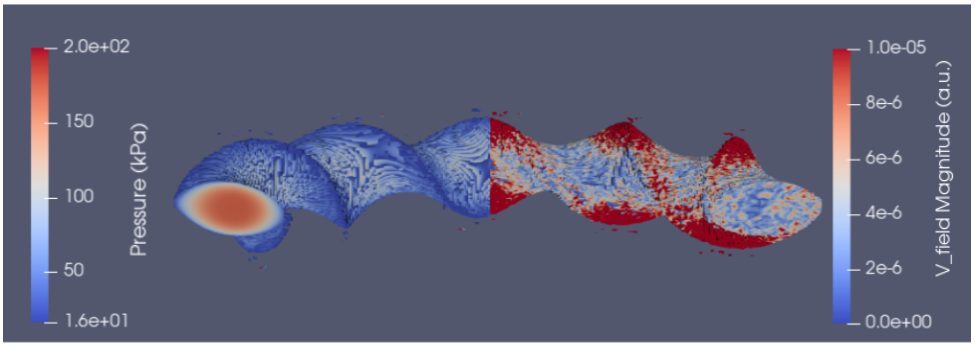

(b) Unstable velocity field (right) and pressure (left) at 10.3 μs

Figure 16: 3D plots of the stellarator showing the different velocity fields and pressure of stable and unstable configurations at the end of their respective simulation

Imposed Flow Case C

Case C is defined by the initial u_0 defined by the half angled sine (eq. 34) with an amplitude of $1x10^{-3}$. Its energy spectrum is shown in figure 14c. For the half angled sine profiled imposed flow, the velocity field is shown in figure 15c.

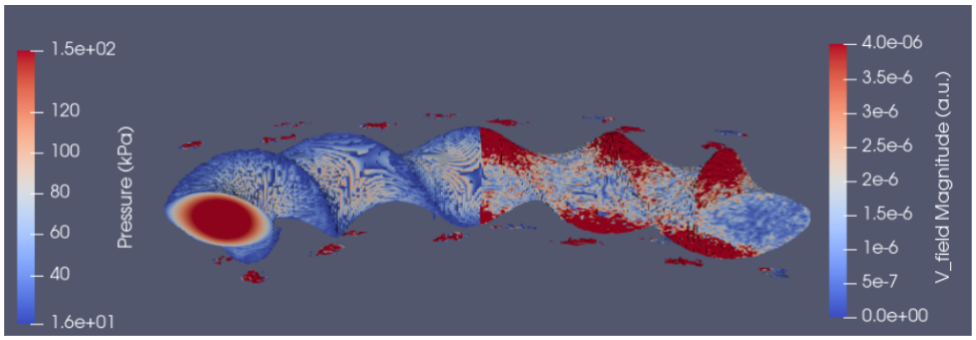

(a) Case A velocity field and pressure profile at 6.6 μs

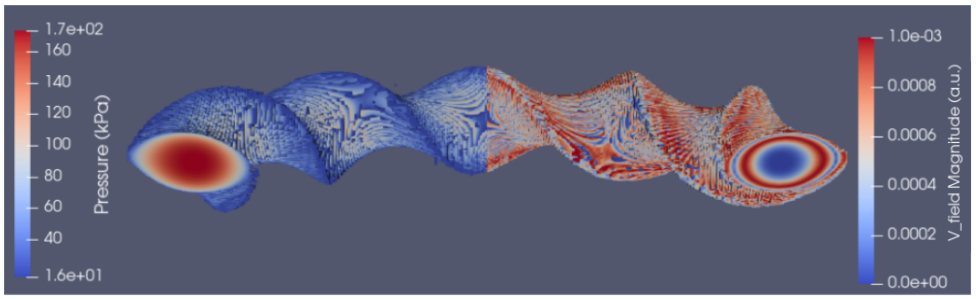

(b) Case B velocity field and pressure profile at 2.9 μs

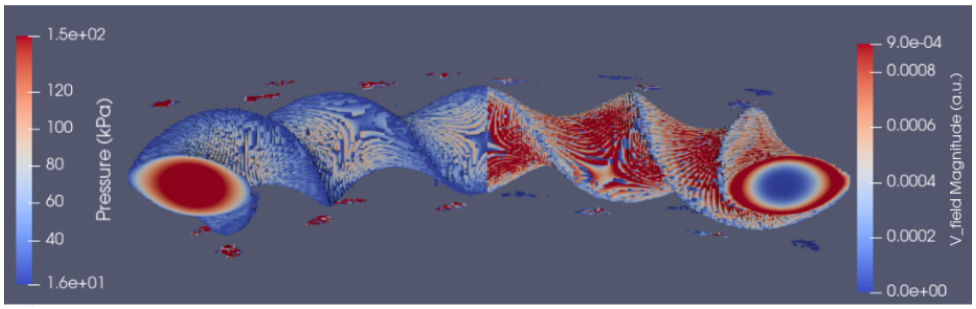

(c) Case C velocity field and pressure profile at 3.3 μs

Figure 17: 3D plots of the stellarator showing the different velocity fields of imposed flow cases at the end of their respective simulation. Velocities are in a.u.

Comparison

The velocity fields and pressure profiles portrayed in figures 14 and 17 show a clear difference in plasma behavior depending on the profile of the shear implemented to impose flow. The velocity profiles change drastically both in shape and in the scale of their values.

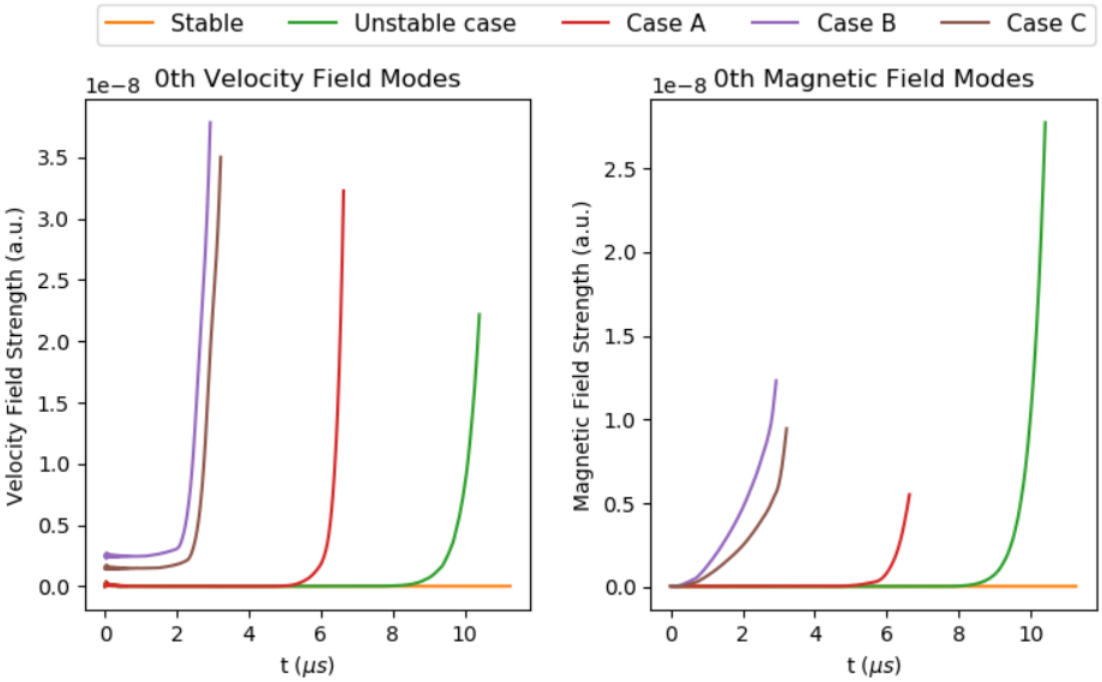

Figure 18: Comparison of 0th mode (m/n=0/0) of velocity and magnetic field spectra between all cases. Velocity and magnetic field spectra are in arbitrary units.

Figure 18 shows the evolution of the 0th toroidal and 0th poloidal mode (m/n = 0/0), meaning the equilibrium component. As expected, from the images it can be seen that the higher amplitude sheared flows visibly shift the velocity spectrum, as these velocities were imposed since the beginning of the simulation. Interestingly, the magnetic field strength quickly rises almost instantly after simulation for the higher amplitude sheared flows.

As shown in figure 18, the mode spectrum of the magnetic field (m/n=0/0) increases in the unstable plasma parameter cases. This is even more starkly observed when comparing cases B and C. Both with the same amplitude, yet case C is slightly more stable due to the profile of the shear used (half angled sine function). Comparing the initial resulting velocity profiles shown in figure 15, although amplitudes are equal for cases B and C, the profile for case B shows that there is one extra ringed area of opposing flow movements. This implies and supports the conclusion that additional shear, at least with the profiles, amplitudes, and configurations simulated in this thesis, act as destabilizing forces.

Gathering the relevant data gives the following table:

Case	Shear Amplitude and Profile	Magnetic Field Time of Increase
Stable	-	$> 11.1\ \mu s$
Unstable	-	$7.5\ \mu s$
Case A	$1x10^{-7}\ (\sin\theta)$	$4.2\ \mu s$
Case B	$1x10^{-3}\ (\sin\theta)$	$0.19\ \mu s$
Case C	$1x10^{-3}\ (\sin\frac{\theta}{2})$	$0.23\ \mu s$

Table 1: Summary table of all cases, their shear amplitudes and cases and the magnetic field time of increase.

From the data shown in table 1 it is clear the introduction of shear in plasma motion prematurely gives rise to early spikes in energy, shortening the general duration of the fusion reaction. Magnetic field modes rise earlier when the shear imposed is of higher amplitudes. There is a clear gap between these two cases, showing the effect and importance of the chosen shear profile.

5 Conclusion and Future Work

For the preparation of this thesis, MIPS code cleaning and merging of several versions was made for the unified future progress of MIPS code development. Additions made include improvement of output management (see Appendix A) and overall adaptation between relevant versions and new equations. Additionally, a private repository shared with interested and qualified parties was created for future collaboration, in the hopes of creating a primary global version which could in turn optimize further developments with MIPS code and nuclear fusion research overall.

Numerical simulations of non-linear MHD in a stellarator plasma have been performed using MIPS code. During the project, the preliminary approach of the implementation of an externally imposed flow in MIPS code has been carried out. Three cases were developed with permutations between shear strength and shear profile type. All imposed flow cases were simulated beginning from an unstable configuration. Analysis of velocity and magnetic field spectra of all cases were conducted with the use of Python scripts and 3D plots were visualized with ParaView software. The analysis shows that the introduction of sheared flow within the plasma causes premature excitation in the linear modes of the magnetic field strength, ultimately causing a more unstable plasma than the non-imposed flow cases.

As a summary of the results, imposing a sheared flow to an unstable configuration with amplitudes of $1\text{x}10^{-7}$ causes magnetic field strength spectra to excite 3.3 μs before the unstable non-imposed flow case. Imposing a stronger sheared flow on the same configuration with an amplitude of $1\text{x}10^{-3}$ causes the magnetic field strength spectra to excite up to 7.4 μs before the unstable non-imposed flow case.

Future Work

For future work, a study of different shear strengths would give more insight into the general effects that shear implementation has on plasma behavior. Those shear flow effects should be investigated not only for the linear stage but also for the non-linear stage of the MHD dynamics.

Most importantly, and particularly for the special case of stellarators, a development of different and more realistic shear flow profiles should be implemented. The profile of the imposed flow should be re-produced from the experiment data in order to compare with the experimental observation.

Furthermore, a self-consistently generated flow can be considered by improving the MHD model, for example, diamagnetic flow and implementing toroidal flow.

Accordingly, the development of MIPS code should be continued to make it capable to perform more advanced and complete MHD model simulations.

6 Acknowledgements

I would like to primarily thank Dr. Shimpei Futatani for all the help, patience, and knowledge provided for the development of this work, this work would have been impossible without him. Also, thanks to Dr. Jordi Marti as well as all the professors and classmates involved in this program for all of the support provided during the entire process. Lastly, I would like to give a big appreciation to the Barcelona Supercomputing Center for having such a valuable resource available for such projects, it was an honor to have had the opportunity of working with this group and with such a renowned facility.

References

[1] W. N. Association, "World energy needs and nuclear power, **https://world-nuclear.org/information-library/current-and-future-generation/world-energy-needs-and-nuclear-power**," 2022.

[2] J. A. de Chalendar and S. M. Benson, "Why 100 percent renewable energy is not enough, **https://www.sciencedirect.com/science/article/pii/s2542435119302144**," *Joule*, vol. 3, no. 6, pp. 1389–1393, 2019.

[3] U. Shahzad, "Global warming: Causes, effects and solutions, **https://www.researchgate.net/publication/316691239_global_warming_causes_effects_and_solutions**," 2015.

[4] "Iter, **http://www.iter.org**."

[5] "Measuring Progress in Fusion Energy: The Triple Product, **https://www.fusionenergybase.com/article/measuring-progress-in-fusion-energy-the-triple-products**."

[6] R. Bilato and R. Kleiber, *IPP Summer University for Plasma Physics, **https://pure.mpg.de/rest/items/item_2146333_1/component/file_2146332/content***. 2012.

[7] R. Matthews, "If the sun is constantly losing mass via nuclear fusion, how come it's not getting any smaller?," 2020.

[8] "Global energy consumption only going up, **https://www.theworldcounts.com/challenges/climate-change/energy/global-energy-consumption**."

[9] EUROfusion, "Fusion On Earth, **https://www.euro-fusion.org/fusion/fusion-on-earth/**."

[10] "Nuclear physics masterclass homepage, university of york, **https://www.york.ac.uk/physics/public-and-schools/nuclear-masterclass-homepage-winter2020/module-3-fusion-winter2020/**."

[11] D. Griffiths, *Introduction to Electrodynamics*. Pearson Education, 2014.

[12] Y. Xu, "A general comparison between tokamak and stellarator plasmas," *Matter and Radiation at Extremes*, vol. 1, no. 4, pp. 192–200, 2016.

[13] "Helically symmetric experiment, **https://hsx.wisc.edu/**."

[14] "Wendelstein 7-x, **https://www.ipp.mpg.de/w7x**."

[15] "Stellar work, **https://www.economist.com/science-and-technology/2015/10/24/stellar-work**."

[16] "Large Helical Device (LHD) project, **https://www-lhd.nifs.ac.jp/pub/lhd_project_en.html**."

[17] S. Murakami, A. Wakasa, H. Maaßberg, C. Beidler, H. Yamada, K. Watanabe, L. E. Group, *et al.*, "Neoclassical transport optimization of lhd," *Nuclear Fusion*, vol. 42, no. 11, p. L19, 2002.

[18] J. Freidberg, *Plasma Physics and Fusion Energy*. Cambridge University Press, 2008.

[19] P. A. Davidson, *An Introduction to Magnetohydrodynamics*. Cambridge Texts in Applied Mathematics, Cambridge University Press, 2001.

[20] V. Nakariakov, "Magnetohydrodynamics (MHD)," p. 42.

[21] A. Singh, S. Banerjee, I. Bandyopadhyay, D. Sharma, S. Jha, R. Srinivasan, R. Daniel, and M. Gopalakrishna, "Modeling of eddy current distribution in the sst-1 tokamak," *Fusion Engineering and Design*, vol. 127, pp. 216–225, 2018.

[22] "Marenostrum, **https://www.bsc.es/marenostrum/marenostrum**."

[23] Y. Todo, N. Nakajima, M. Sato, and H. Miura, "Simulation study of ballooning modes in the large helical device," *Plasma and Fusion Research*, vol. 5, pp. S2062–S2062, 2010.

[24] Y. Suzuki, S. Futatani, and J. Geiger, "Nonlinear MHD simulation of core plasma collapse events in wendelstein 7-x," *Plasma Physics and Controlled Fusion*, vol. 63, no. 12, p. 124009, 2021.

[25] S. Futatani and Y. Suzuki, "Non-linear magnetohydrodynamic simulations of plasma instabilities from pellet injection in large helical device plasma," *Plasma Physics and Controlled Fusion*, vol. 61, no. 9, p. 095014, 2019.

[26] K. Ichiguchi, Y. Suzuki, M. Sato, Y. Todo, T. Nicolas, S. Sakakibara, S. Ohdachi, Y. Narushima, and B. Carreras, "Three-dimensional MHD analysis of heliotron plasma with RMP," *Nuclear Fusion*, vol. 55, no. 7, p. 073023, 2015.

[27] W. E. Amatucci, D. N. Walker, G. Ganguli, J. A. Antoniades, D. Duncan, J. H. Bowles, V. Gavrishchaka, and M. E. Koepke, "Plasma response to strongly sheared flow," *Phys. Rev. Lett.*, vol. 77, pp. 1978–1981, 1996.

[28] P. W. Terry, "Suppression of turbulence and transport by sheared flow," *Rev. Mod. Phys.*, vol. 72, pp. 109–165, 2000.

[29] C. Holland, J. H. Yu, A. James, D. Nishijima, M. Shimada, N. Taheri, and G. R. Tynan, "Observation of turbulent-driven shear flow in a cylindrical laboratory plasma device," *Phys. Rev. Lett.*, vol. 96, p. 195002, 2006.

A MIPS file management

A brief description of all the relevant input and output files is presented with the ends of providing an organized manual for future reference and work:

Compilation File

The file holding the instructions for the compilation of MIPS code is called '`Makefile`'. Within these instructions there must be indicated the type of field to be used, whether or not Boozer coordinates are to be used, and the resolution for the calculations within the program.

Input Parameters

The input parameters of the simulation are declared within the file named '`input_parameters`'. The variables to be declared within are:

- `JOB_SEQ`: Integer denoting the job number
- `KSTEP`: Starting step of the simulation
- `KSMAX`: Maximum step the simulation can reach
- `ETLIM`: Maximum simulation time to be reached
- `KWCHK`: Number of steps to which output data is written (if set to 100, for example, output data of the simulation will be written at ksteps 0, 100, 200, 300, and so on)
- `KWOUT`: Number of steps to which .rst files will be created, similar to the `KWCHK` variable
- `KSNAPSH`: Number of steps to which 2D poloidal plane data is written
- `KMOVIE`: Number of steps to which data is stored to create a movie of the evolution of the plasma
- `DT`: t_{MIPS}, the assigned internal time value for each step
- `NUO`: Viscosity
- `ETAO`: Resistivity
- `NU_NO`: Diffusivity of density
- `CHIO`: Perpendicular thermal diffusivity
- `CHIO_PARALLEL`: Parallel thermal diffusivity
- `PERTURB_TYPE`: Type of perturbation to be used within the simulation
- `flag_HM`: A boolean setting if the Hazeltime-Meiss extended MHD model is used within the simulation
- `VAC_TYPE`: Sets the vacuum type for the simulation

- `FIELD_TYPE`: Sets the type of field to be used
- `PELLET`: Sets if pellet injection is used or not within the simulation
- `MACHINE`: Sets geometry of the reactor

Input Field

The file '`field_ASDEX`' and '`input_field`' are unformatted input files holding variables describing ASDEX or non-ASDEX type of fields to be implemented within the simulation. These were included within several clauses of the code depending if the variable '`FIELD_TYPE`' within the '`input_parameters`' file is indicated as '`ASDEX`' or not. The variables describe the dimensions of the field in cylindrical coordinates as well as imposed pressure, magnetic field, and resistivity.

Boozer Input

The file '`input_boozer`' is an unformatted input file which holds the information required for establishing Boozer coordinates. Whether or not these coordinates are used is established in several clauses within the code dependent on a variable declared within '`Makefile`'.

Energies output

The output calculated energies are shown in the output file `energies` as follows:

- `kstep`: Integer showing simulation step value at which row data is shown.
- `wat`: Power in Watts at current kstep.
- `kin_energy`: Kinetic Energy. Calculated as shown in equation 23.
- `mag_energy`: Magnetic Energy. Calculated as shown in equation 24.
- `thr_energy`: Thermal Energy. Calculated as shown in equation 25.
- `total_energy`: Total Energy. Calculated as shown in equation 26.

Furthermore, the energies spectrum is outputted to the file `energies_spectrum` in a similar fashion showing the step, power, and modes from one to twenty of the energies (`kstep, wat, e_n=0, e_n=1, e_n=2,...`).

Spectrum Variables

The output file `spectrum_variables` contains the output spectrum information for the velocity field, magnetic field, and pressure at the different steps of the simulation. Here, the output has the following structure:

- `kstep`: Integer showing simulation step value at which row data is shown.

- `t`: t_{MIPS}, the internal un-normalized MIPS time. Equal to `kstep` times `DT`, the latter being declared in the `input_parameters` file.
- `vrad_spec_ij`: Velocity field spectra. Integer i denotes the poloidal mode (commonly referred to as m) and j the toroidal mode (referred to as n). The output goes from one to three for each integer, except for the equilibrium modes which only have m/n = 0/0 and m/n = 0/1, hence the output goes as `vrad_spec_00, vrad_spec_01, vrad_spec_11, vrad_spec_12, vrad_spec_13, vrad_spec_21, vrad_spec_22,..., vrad_spec_33`
- `brad_spec_ij`: Magnetic field spectra. Shown as the velocity field spectra is shown.
- `prs_spec_ij`: Pressure spectra. Shown as the velocity field spectra is shown.

Pellet Injection Information

If the simulation takes into account pellet injection to mitigate edge localized modes (ELMs), a major cause for plasma energy loss and instabilities, then the output file `pellet_info` outputs the relevant pellet information as `kstep, dt, pellet_R, pellet_particle, ablation_rate`.

Simulation Output

The ongoing status of the running simulation yields tracking output into the file `output_data` with data regarding simulation and processing times as well as used field parameters.

2D Imaging

For creating 2D snapshots of the different recorded, calculated slices of the plasma, the output file `variables2D_poloidal` holds this data in an unformatted structure.

Total Variables

Important miscellaneous variables of the ongoing simulation are outputted in an unformatted fashion unto the output file `total_variables`. The variables are outputted as `kstep, t, rho_psi, xiota_psi, vrad_total, brad_total, prs_total` where `rho_psi, xiota_psi` are variables regarding Boozer coordinate grid point tracking.